Portable High-Sensitivity Raman-Electrochemical Microsensor Utilizing Polarization Shift Strategy for Anti-Interference Detection of 5-Hydroxytryptamine

Ruwei Liu[a,1], Yuyang He[b,1], Fan Zhao[a], Yunhan Ling[a,*], Xiaoming Yuan[b], Shilin Li[a], Zhengjun Zhang[a,*]

[1] Ruwei Liu and Yuyang He contributed equally to this work (co-first author)

[a] *Lab of Advanced Materials, School of Materials Sciences and Engineering, Tsinghua University, Beijing 100084, PR China*

[b] *School of Science, China University of Geosciences, Beijing 100083, PR China*

*Corresponding authors:

E-mail address: yhling@mail.tsinghua.edu.cn (Y. Ling), zjzhang@tsinghua.edu.cn (Z. Zhang).

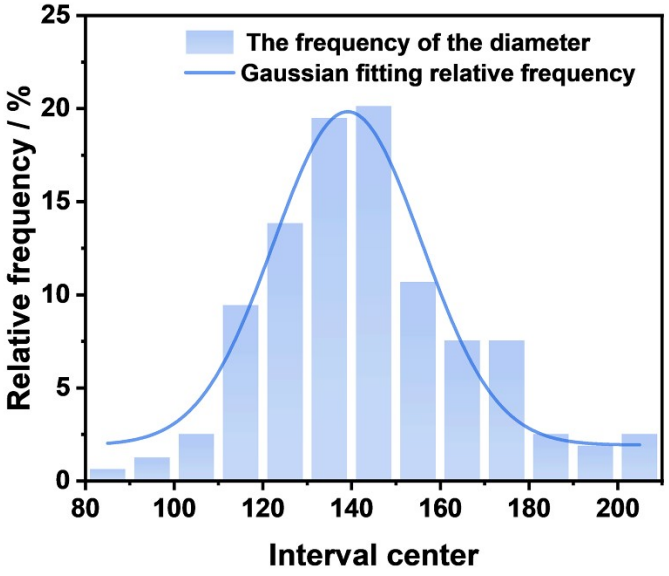

Fig. S1 Analysis of the particle size distribution of gold nanoparticles.

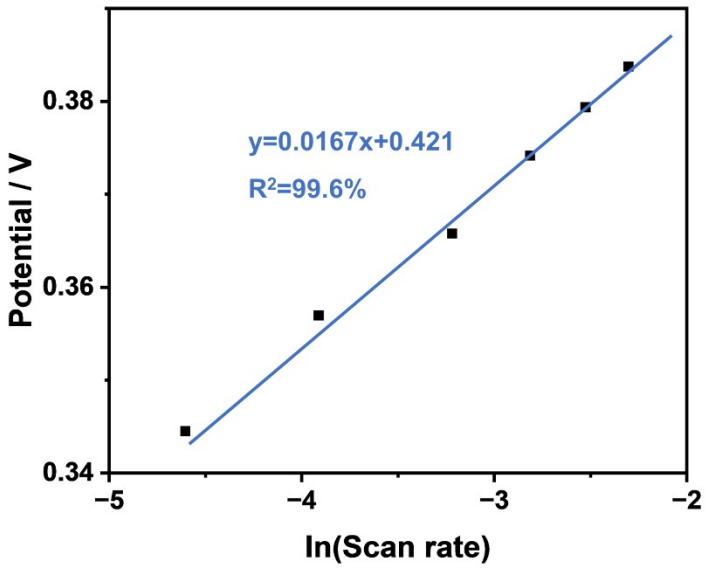

Fig. S2 The linear relationship between the ln function of the scanning speed and the potential.

1 Optimization of experimental parameters

1.1 Polarization Time

As the polarization time increases, the amount of 5-HT adhering to the sensor increases, thereby improving the detection performance, as shown in Figs. S3a and

S3b. As the polarization time increases, the oxidation peak current generated by 5-HT also increases. However, when the polarization time reaches 120 seconds, the rate of increase slows down. Therefore, to avoid excessive detection time, we selected 120 seconds as the optimal polarization time.

1.2 Stirring Speed

During the stirring process with a stir bar, increasing the stirring speed increases the amount of 5-HT adhering to the sensor in the solution. Researchers investigated the effect of stirring speed on detection, with results shown in Figs S3c and S3d. Without stirring, the detection level remains at a low state. As stirring speed increases, the oxidation peak current of 5-HT also rises. Considering the risk of splashing at high speeds, 600 rpm was selected as the optimal stirring speed.

1.3 Polarization Voltage

During the polarization process, polarization voltage is a crucial variable. We controlled the polarization voltage to generate a negative potential on the sensor surface, enabling positively charged 5-HT in the solution to adsorb onto the sensor surface. The open-circuit potential at this point is 0.25 V vs. Ag/AgCl. Researchers investigated the effect of polarization voltage on detection, with results shown in Figs S3e and S3f. It can be observed that within the polarization voltage range of 0.3 V to -0.1 V, the oxidation peak current of 5-HT exhibits a stepwise increase. Considering that a low polarization voltage may increase costs, we selected 0 V as the optimal polarization voltage.

1.4 Number of polymerization cycles in chlorogold acid solution

By using scanning CV to polymerize gold nanoparticles, the LSPR effect is realized on the sensor surface to enhance the electromagnetic field and achieve the Raman enhancement effect. Therefore, different numbers of polymerization cycles result in different quantities of gold nanoparticles polymerized on the sensor surface. We performed Raman detection on sensors with scanning cycles of 10, 20, 30, and 40 cycles. The results are shown in Figs S4a and S4b. SEM observations of the surface morphology of these four sensors were also conducted to assist in selecting the optimal number of cycles. Surface morphology images are shown in Fig S5a-h. We can observe that as the number of scanning cycles increases, the Raman signal exhibits an increasing trend. By combining this with the SEM morphology, we made our selection. After 30 cycles, the Raman signal did not show a significant increase, and SEM images revealed that at 30 cycles, gold nanoparticles had almost completely covered the laser-induced graphene surface. Therefore, we selected 30 cycles as the optimal number of polymerization cycles.

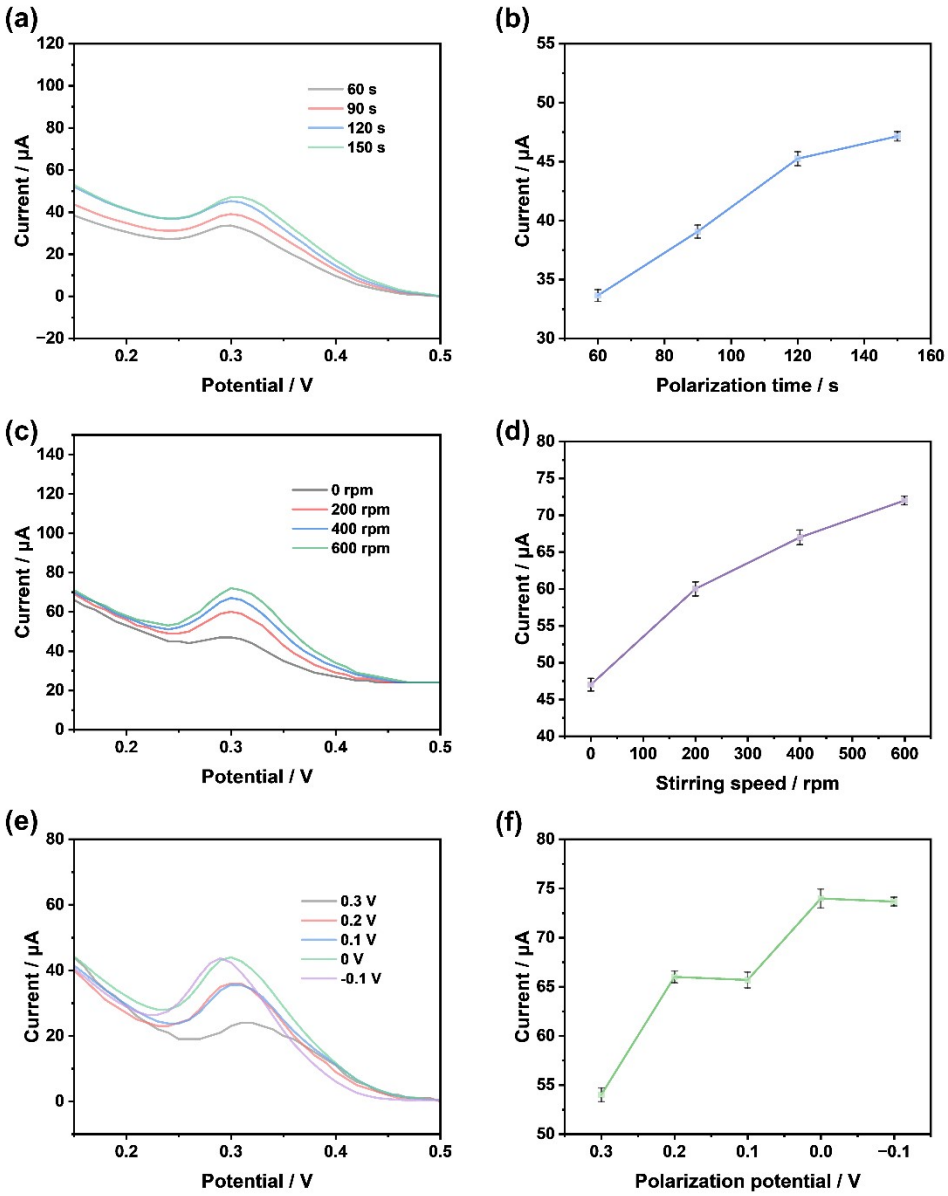

Fig. S3 (a) Comparison of DPV signals of 5-HT at different polarization times. (b) Comparison of peak currents of 5-HT at different polarization times. (c) Comparison of DPV signals of 5-HT at different stirring times. (d) Comparison of peak currents of 5-HT at different stirring times. (e) Comparison of DPV signals of 5-HT at different polarization potentials. (f) Comparison of peak currents of 5-HT at different polarization potentials.

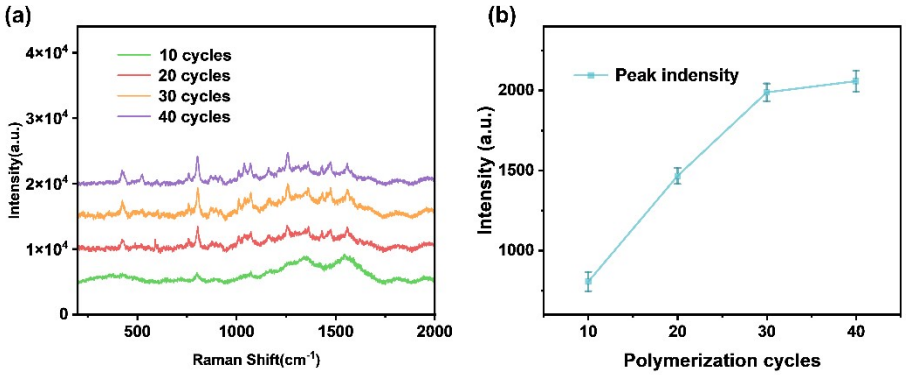

Fig. S4 (a) Raman spectroscopy of 5-HT on sensors with different numbers of polymerization rings. (b) Comparison of peak intensities at different circle numbers.

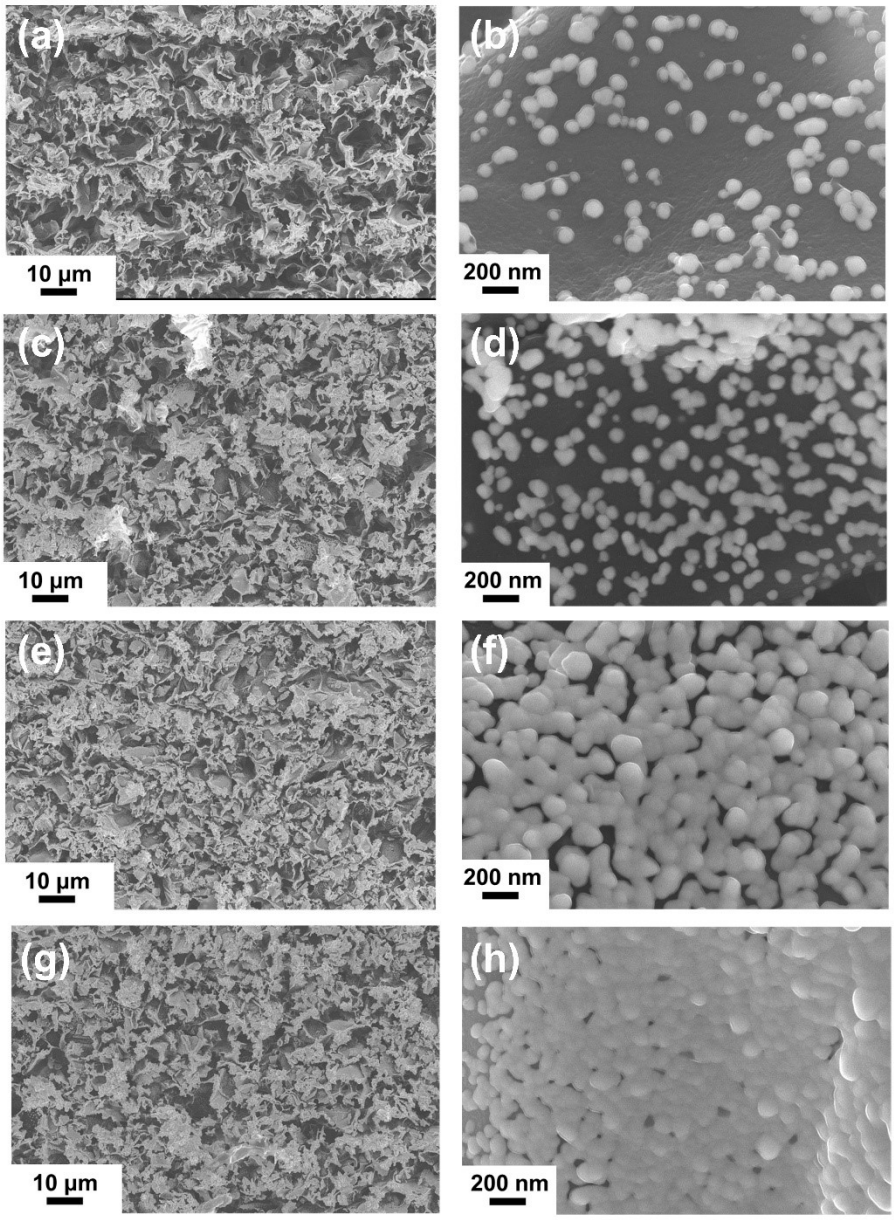

Fig. S5 (a, b) SEM of A-Au/LIG ten-circle sensor. (c, d) SEM of A-Au/LIG twenty-circle sensor. (e, f) SEM of A-Au/LIG thirty-circle sensor. (g, h) SEM of A-Au/LIG forty-circle sensor.

Table S1. Comparison of the performance of previously reported sensors with A-Au/LIG.

Sensor	Materials Used	Detection Range / μM	LOD / nM	Ref.
Graphene-Based Sensor	AuNRTs-rGO, AuNPs, GCE	3–1×10^3	387	[1]
Metal-Based Nanoparticles Sensor	CP-AuNPs, GCE	10–320	5700	[2]
Serotonin Detection with CNTs	Benzofuran derivative-functionalized MWCNTs	5.0–900.0	2000	[3]
Metal-Based Nanoparticles Sensor	PdNP:MWCNT, GCE	2–400	77	[4]
Metal-Based Nanoparticles Sensor	MnO2-GR, GCE	0.1–800	10	[5]
Carbon spheres/GCE	Carbon spheres/GCE	40–750	700	[6]
Glassy carbon electrode	GCE/P-Arg/ErGO/Au NP	0.01–0.5, 1–10	30	[7]
platinum electrode	PEDOT	20–100	71	[8]
carbon electrode	A-Au/LIG	0.005-50	2.23	This work

2 Selective Supplementary Analysis

To comprehensively evaluate the selectivity of the A-Au/LIG sensor, we systematically investigated the interference from common substances such as dopamine (DA), ascorbic acid (AA), adrenaline (AD), and noradrenaline (NA). As shown in Fig. S6 a, c, e, g, when only 5 μM of these interferents was present, their oxidation signals were effectively suppressed after the polarization transfer, with a residual signal of less than 2% for each. More critically, in complex systems where 5-HT (500 nM) coexisted with each interferent (5 μM), the DPV signal retention rate for 5-HT remained above 95% (Fig. S6 b, d, f, h). These results conclusively demonstrate that our developed polarization-transfer strategy can universally mitigate the interference from a variety of species, ensuring the high selectivity of the sensor towards 5-HT detection.

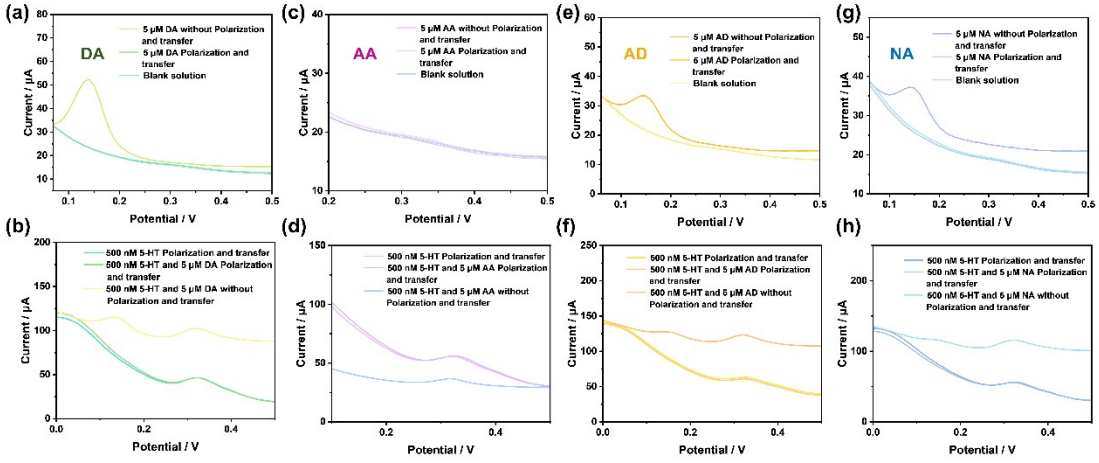

Fig. S6 Anti-interference detection of 5-HT. DPV responses of the A-Au/LIG sensor in the presence of common interferents (DA, AA, AD, NA) before and after the polarization transfer. (a) In the presence of 5 μM DA, the DPV plots before and after transfer were compared with those of the blank solution. (b) The DPV images before and after transfer in the presence of 5 μM DA and 500 nm 5-HT were compared with those in the presence of only 500 nm 5-HT solution. (c) In the presence of 5 μM AA, the DPV plots before and after transfer were compared with those of the blank solution. (d) The DPV images before and after transfer in the presence of 5 μM AA and 500 nm 5-HT were compared with those in the presence of only 500 nm 5-HT solution. (e) In the presence of 5 μM AD, the DPV plots before and after transfer were compared with those of the blank solution. (f) The DPV images before and after transfer in the presence of 5 μM

AD and 500 nm 5-HT were compared with those in the presence of only 500 nm 5-HT solution. (g) In the presence of 5 μM NA, the DPV plots before and after transfer were compared with those of the blank solution. (h) The DPV images before and after transfer in the presence of 5 μM NA and 500 nm 5-HT were compared with those in the presence of only 500 nm 5-HT solution.

3 UPLC-MS/MS Analysis

3.1 Experimental conditions

Ultra-high performance liquid chromatography tandem mass spectrometry (UPLC-MS/MS) analysis was conducted on a system consisting of a Waters ACQUITY UPLC I-Class and a SCIEX QTRAP 4500 triple quadrupole linear ion trap mass spectrometer for cross-validation of the detection results.A 50 μL aliquot of each spiked biological sample was protein-precipitated with 200 μL of acetonitrile/methanol (1:1, v/v) containing 0.1% formic acid, followed by centrifugation at 13,000 rpm for 10 min. Subsequently, 180 μL of the supernatant was transferred to a clean 1.5 mL centrifuge tube and centrifuged again under the same conditions for an additional 10 min. Finally, 150 μL of the resulting supernatant was collected into a clean vial for UPLC-MS/MS analysis.Chromatographic separation was performed on a Waters XSelect HSS T3 column (2.5 μm, 2.1 × 100 mm) maintained at 40 °C. A binary gradient elution program was employed, using acetonitrile/methanol as mobile phase A and 0.1% formic acid in water as mobile phase B, at a flow rate of 0.3 mL/min. The eluted samples were ionized under the following optimized mass spectrometric conditions: ionization mode: positive; spray voltage: 5.5 kV; source temperature: 550 °C; curtain gas: 30 psi; declustering potential: 60 V; collision energy: 15 V. Data acquisition was performed in selected reaction monitoring (SRM) mode.

3.2 Results

Analyst Software 1.6.4 was used for compound information acquisition and MultiQuant 3.0.3 was used for data analysis.

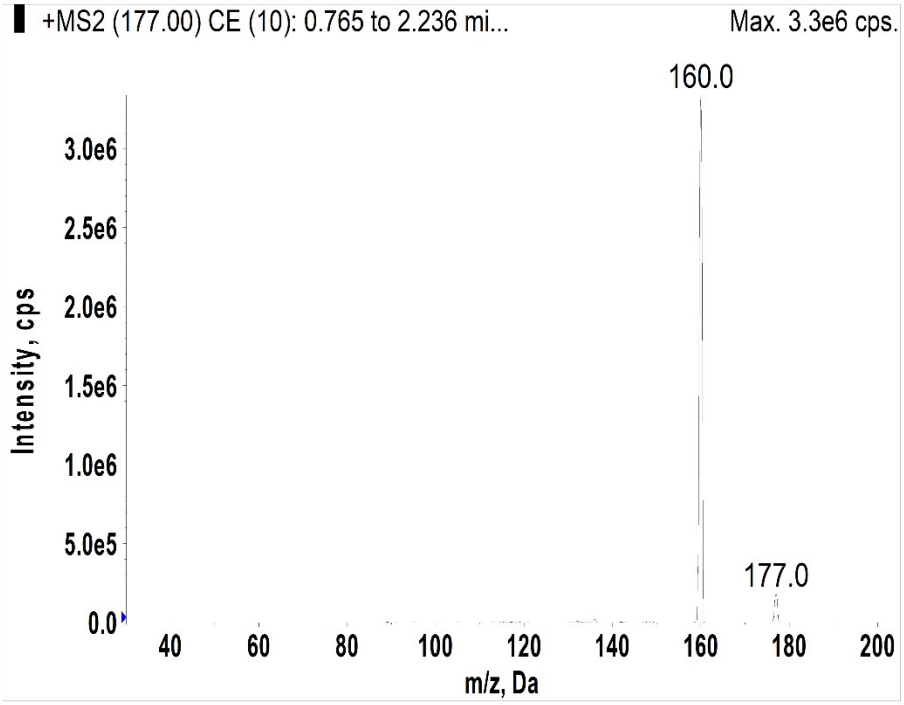

Figure S7 Secondary mass spectrum of 5-HT

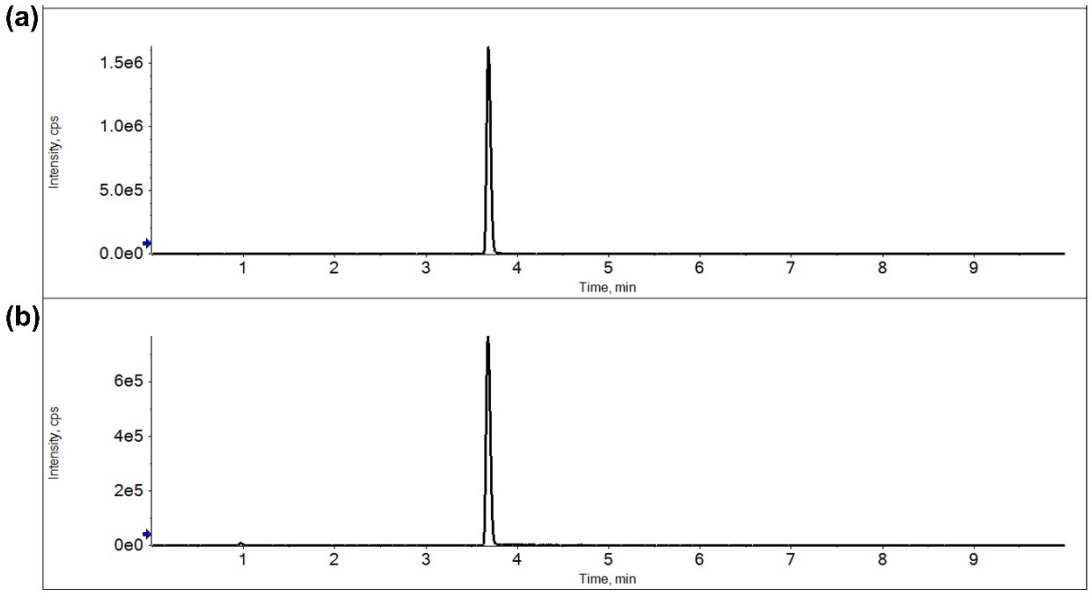

Figure S8 (a) Chromatogram of standard 5-HT. (b) Chromatogram of a serum sample spiked with 50 nM 5-HT

1. K. Mahato, B. Purohit, K. Bhardwaj, A. Jaiswal and P. Chandra, *Biosensors and Bioelectronics*, 2019, **142**, 111502.
2. S. A. Leau, C. Lete, C. Matei and S. Lupu, *Journal*, 2023, **13**.
3. M. Mazloum-Ardakani and A. Khoshroo, *Journal of Electroanalytical Chemistry*, 2014, **717-718**, 17-23.
4. N. Kumar, Rosy and R. N. Goyal, *Sensors and Actuators B: Chemical*, 2017, **239**, 1060-1068.
5. L. Nehru, S. Chinnathambi, E. Fazio, F. Neri, S. G. Leonardi, A. Bonavita and G. Neri, *Journal*, 2020, **10**.
6. J. Zhou, M. Sheng, X. Jiang, G. Wu and F. Gao, *Journal*, 2013, **13**, 14029-14040.
7. M. Z. H. Khan, X. Liu, Y. Tang, J. Zhu, W. Hu and X. Liu, *Microchimica Acta*, 2018, **185**, 439.
8. N. F. Atta, A. Galal and R. A. Ahmed, *Journal of The Electrochemical Society*, 2011, **158**, F52.